Eur. Phys. J. B **34**, 409–413 (2003)
DOI: 10.1140/epjb/e2003-00238-8

THE EUROPEAN PHYSICAL JOURNAL B

Symmetry, phonons and rigid-layers modes in commensurate double wall carbon nanotubes

E. Dobardžić[a], I. Milošević, T. Vuković, B. Nikolić, and M. Damnjanović

Faculty of Physics, University of Belgrade, POB 368, 11001 Belgrade, Serbia and Montenegro

Received 2 May 2003 / Received in final form 19 June 2003
Published online 9 September 2003 –

Abstract. For translationally periodic double-wall carbon nanotubes stable configurations and full symmetry groups are determined. Using this, the phonon dispersions and eigenvectors are calculated and assigned by the complete set of conserved quantum numbers. In particular, the modes corresponding to the relative coaxial motions of the rigid layers are studied in the context of low inter-wall interaction.

PACS. 63.22.+m Phonons or vibrational states in low-dimensional structures and nanoscale materials – 61.46.+w Nanoscale materials: clusters, nanoparticles, nanotubes, and nanocrystals – 78.30.Na Fullerenes and related materials

Since the discovery by Iijima [1], carbon nanotubes (CNs), have been investigated intensively. Due to their numerous potential applications, the achievement of the high yield production (at low cost) with well controlled chirality, diameter and number of layers is a goal of many research groups. Recently, double-walled CNs (DWCNs) have been generated by coalescence of "bucky-peapods" encapsulated into single-walled CNs [2] and a path to large scale synthesis has been reported [3]. Also, DWCNs production by chemical vapor deposition have been achieved [4]. Resonant Raman measurements have been used to determine the inner and outer diameter of the DWCNs by identifying the radial breathing modes and high energy modes [5]. Breathing-like phonon modes of DWCNs have been studied theoretically [6]. The symmetry breaking arguments are used to predict the low interaction between the walls [7,8], the effect which has been verified numerically [9,10] and experimentally [11].

A far as we know, no systematic theoretical study of the DWCNs stable configurations, symmetry and lattice dynamics has been reported yet. Here we find the stable configurations and symmetry groups of the translationally periodic, *i.e.* commensurate DWCNs (CDWCNs) and calculate their phonon dispersions and atomic displacements. Then we turn to the inspection of the low energy optic modes, which describe the relative coaxial motion of almost rigid layers, giving an additional evidence of the inter-wall interaction. The calculations were performed by means of the code *POLSym* (E) [12]: based on the line (rod or monoperiodic) groups symmetry [13], it is maximally efficient for studies of the systems periodical in one direction, including CDWCNs.

[a] e-mail: edib@ff.bg.ac.yu

Symmetry group of SWCN [7] is a line group $\boldsymbol{L}$; it is $\boldsymbol{T}_q^r(a)\boldsymbol{D}_n$ for chiral ($\mathcal{C}$) and $\boldsymbol{T}_{2n}^1(a)\boldsymbol{D}_{nd}$ for achiral (zig-zag, $\mathcal{Z}$ and armchair, $\mathcal{A}$) tubes. The orders of the principle axes of the line and its isogonal group are $n = \mathrm{GCD}(n_1, n_2)$ and q, a is translational period and r is helicity parameter of the screw axis $\boldsymbol{T}_q^r(a)$ generated by $(C_q^r|na/q)$ (especially, $\boldsymbol{T}_n^0(a) = \boldsymbol{T}(a)$ is pure translational group). The roto-translational operations (rotations around the tube axis and screw axis) comprise the first family subgroup [13] $\boldsymbol{L}^{(1)} = \boldsymbol{T}_q^r(a)\boldsymbol{C}_n$ of $\boldsymbol{L}$. Additional parities are U-axis (rotations for 180° around the axis perpendicular to the tube), and in achiral tubes only, horizontal and vertical mirror and glide planes. The spatial inversion transforms the tube (n_1, n_2) into (n_2, n_1): a $\mathcal{C}$ tube with right chirality ($n_1 > n_2 > 0$, chiral angle $\theta \in (0, 30°)$) becomes the tube with left chirality $\theta \in (0, -30°)$, while achiral tubes remain identical. Left and right counterparts have either the same (*e.g.* vibrational) or directly related properties (*e.g.* opposite rotation of the polarization of light). Their symmetry parameters q, n and a are the same, while the helicity parameters satisfy $r_{\mathrm{right}} + r_{\mathrm{left}} = q$.

CDWCN W@W′ is a pair of coaxial single-layer tubes with commensurate translational periods: W$= (n_1, n_2)$ is nested within W′ $= (n_1', n_2')$. Spatial inversion relates the right-right CDWCN $(n_1, n_2)@(n_1', n_2')$ to the left-left one $(n_2, n_1)@(n_2', n_1')$. Thus, if both layers are chiral, together with the right-right tube the right-left one $(n_1, n_2)@(n_2', n_1')$ should be considered independently. We studied 318 CDWCNs selected as follows: all of 1280 right SWCNs with diameters 2.8 Å $\leq D \leq$ 50 Å are taken as the inner wall W, while the outer wall W′ may be any SWCN with [1] $D' = D + \Delta$, 6.48 Å$\leq \Delta \leq$ 7.28 Å. There

Table 1. Series of CDWCNs with colinear chiral vectors and their right-left counterparts. The tubes of the series in Column 1 have the considered diameters (outer wall 9.6 Å $\leq D \leq$ 50 Å) for the values of n given in the Column 4; the values in brackets should be omitted. Corresponding line and isogonal group are in the columns 2 and 3. The translational periods are given with the length unit $a_0 = 2.46$ Å.

CDWCN ray	Line Group	Isogonal	n
$(1,0)n@(n+9)$	$\boldsymbol{T}(\sqrt{3})\boldsymbol{D}_{1d}$	$\boldsymbol{D}_{1d}$	$^{4,5,\ldots,62}_{(6,9,12,\ldots,60)}$
	$\boldsymbol{T}(\sqrt{3})\boldsymbol{D}_{3d}$	$\boldsymbol{D}_{3d}$	$^{6,9,12,\ldots,60}_{(9,18,\ldots 54)}$
	$\boldsymbol{T}(\sqrt{3})\boldsymbol{D}_{9d}$	$\boldsymbol{D}_{9d}$	$18, 27 \ldots, 63$
	$\boldsymbol{T}_c(\sqrt{3})\boldsymbol{S}_{18}$		9
$(1,1)n@(5+n)$	$\boldsymbol{T}(1)\boldsymbol{D}_{1d}$	$\boldsymbol{D}_{1d}$	$^{2,3,\ldots,36\ (5,10,}_{15,20,25,30,35)}$
	$\boldsymbol{T}(1)\boldsymbol{D}_{5d}$	$\boldsymbol{D}_{5d}$	$10, 15, \ldots, 35$
	$\boldsymbol{T}_c(1)\boldsymbol{S}_{10}$		5
$^{(3,2)n@(n+2)}_{(2,3)n@(n+2)}$	$\boldsymbol{T}^1_2(\sqrt{57})\boldsymbol{D}_1$	$\boldsymbol{D}_2$	$1, 3, \ldots, 13$
	$\boldsymbol{T}(\sqrt{57})\boldsymbol{D}_2$		$2, 4, \ldots, 14$
$^{(4,1)n@(n+2)}_{(1,4)n@(n+2)}$	$\boldsymbol{T}^1_2(\sqrt{7})\boldsymbol{D}_1$	$\boldsymbol{D}_2$	$^{1,3,\ldots,13}_{1,3,\ldots,11}$
	$\boldsymbol{T}(\sqrt{7})\boldsymbol{D}_2$		$^{2,4,\ldots,12}_{2,4,\ldots,12\ (6)}$
	$\boldsymbol{T}^3_{14}(\sqrt{7})\boldsymbol{D}_1$	$\boldsymbol{D}_{14}$	$\bar{}_{13}$
	$\boldsymbol{T}^{13}_{14}(\sqrt{7})\boldsymbol{D}_2$		$\bar{}_{6}$
$^{(7,3)n@(n+1)}_{(3,7)n@(n+1)}$	$\boldsymbol{T}(\sqrt{237})\boldsymbol{D}_1$	$\boldsymbol{D}_1$	$1, 2, \ldots, 7$
$^{(8,1)n@(n+1)}_{(1,8)n@(n+1)}$	$\boldsymbol{T}(\sqrt{219})\boldsymbol{D}_1$	$\boldsymbol{D}_1$	$1, 2, \ldots, 7$

are 42236 different such right-right DWCNs. However, only 240 among them are commensurate. Both walls are chiral in 78 of them, and their right-left counterparts are to be added, giving a sample of 318 commensurate DWCNs. It is interesting that out of firstly selected 1280 SWCNs only 207 (out of which 98 are chiral) appear as the layers of CDWCNs. More than half of all CDWCNs, namely 178 tubes, are with the colinear chiral vectors $n(\hat{n}_1, \hat{n}_2)$ and $n'(\hat{n}_1, \hat{n}_2)$ ($\hat{n}_i = n_i/n = n'_i/n'$, $i = 1, 2$) of the ingredient layers. These series of tubes we denote shortly as $(\hat{n}_1, \hat{n}_2)n@n'$ and $(\hat{n}_2, \hat{n}_1)n@n'$ for the right-left counterpart. Within this class there are 60 zig-zag $\mathcal{ZZ}_n = (1,0)n@(n+9)$, and 35 armchair, $\mathcal{AA}_n = (1,1)n@(n+5)$, Table 1.

Symmetry transformations of DWCN leave both layers invariant. Thus, DWCN symmetry group is the intersection of the groups of the layers. In contrast to the roto-translational symmetries, parities depend on the relative layers positions, which are parameterized by two coordinates. Let x- and x'-axis pass through the centers of carbon hexagons of W and W′ (layers z- and z'-axis coincide). The angle of rotation Φ and length of translation Z (around and along the tube axis, respectively), which are to be performed on x to match x', completely parameterize relative walls position.

Roto-translational symmetries of $(n_1, n_2)@(n'_1, n'_2)$ form line group [7]: $\boldsymbol{L}^{(1)}_{\mathrm{WW}'} = \boldsymbol{T}^R_Q(A)\boldsymbol{C}_N$. It is generated by C_N and the helical generator $(C^R_Q|NA/Q)$, with the parameters determined by the layers' ones:

$$N = \mathrm{GCD}(n, n'), \quad A = \hat{a}'a = \hat{a}a', \tag{1}$$

$$Q = N\sqrt{\tilde{q}\tilde{q}'}/\tau, \qquad R = (r\hat{a}\tau + s\tilde{q})Q/q.$$

Here, $\tilde{q} = q/n$, $\tilde{q}' = q'/n'$, $\tau = \sqrt{\tilde{q}\tilde{q}'}/\mathrm{GCD}(\frac{r\hat{a}'n' - r'\hat{a}n}{N}, \sqrt{\tilde{q}\tilde{q}'})$, $s = \tau(r\hat{a}q' - r'\hat{a}'q)(\hat{n}^{\phi(\hat{n}')} - 1)/n'\tilde{q}\tilde{q}'$ (ϕ is Euler function), $\hat{a}' = \sqrt{\tilde{q}'/\mathrm{GCD}(\tilde{q}, \tilde{q}')}$, $\hat{a} = \sqrt{\tilde{q}/\mathrm{GCD}(\tilde{q}, \tilde{q}')}$. Any integer $R + jQ/N(\mathrm{mod}Q)$ ($j = 1, \ldots, N$) may be equivalently used; we chose for R the unique one which is nonnegative, less than Q and co-prime to it.

The parities pertain to the DWCN symmetry group only for the special positions of the constituent SWCNs, where their U-axes and/or mirror planes coincide. The topological argument [14] predicts that the extremes, including the stable configuration, of the interaction potential $V(\Phi, Z) = \frac{1}{2}\sum v(\boldsymbol{r}_\alpha - \boldsymbol{r}_{\alpha'})$ (summation over all atoms α of W and α' of W′) are in the most symmetrical positions. As there are several physically different highly symmetric special positions, the stable configurations are singled out numerically. The calculations are performed using the inter-atomic potential v of the Lenard-Jones type [15]. It turns out that $V(\Phi, Z)$ is not very sensitive to small variations of the inter-layer distance around minimum at approximately 3.44 Å. Thus the influence of the radial relaxation of the walls is too small to affect equilibrium positions: the topologically allowed stable positions form a discrete set, and a weak relaxation cannot switch between them. Thus, we assume the layers of the CDWCN retain (isolated) single-wall tube geometry. This determines the interlayer distance 3.44 Å± 0.2 Å, as explained before.

The unique global minimum of $V(\Phi, Z)$ is found, in accordance with the topological argument, in the configuration with the highest symmetry. Whenever at least one layer of CDWCN is chiral, the stable configuration is at $(\Phi, Z) = (0, 0)$, with coinciding x- and x'-axis, becoming common U-axis (in addition to $\boldsymbol{L}^{(1)}$). As chiral wall has no mirror/glide planes, this configuration is maximally symmetric. With both achiral walls the only CDWCNs are series of zig-zag, $\mathcal{ZZ}_n$, and armchair $\mathcal{AA}_n$ tubes. For $\mathcal{ZZ}_9$ and $\mathcal{AA}_5$ the minimum is at $(\Phi, Z) = (\pi/2Q, a/4)$ for $\mathcal{ZZ}_9$ and $\mathcal{AA}_5$, while in all other cases $(\Phi, Z) = (0, a/4)$. The straightforward inspection (see Fig. 1) shows that besides the common U axis and horizontal roto-reflection plane, there appear glide (only in $\mathcal{ZZ}_9$ and $\mathcal{AA}_5$) or vertical mirror planes. We define the DWCN coordinate system taking common U-axis and tube axis as the x- and z-axes. In $\mathcal{ZZ}_n$ and $\mathcal{AA}_n$ tubes, U-axis is perpendicular to the mirror/glide plane (thus it is yz-plane).

Altogether, previously found roto-translational subgroups and the parities in the stable configurations form

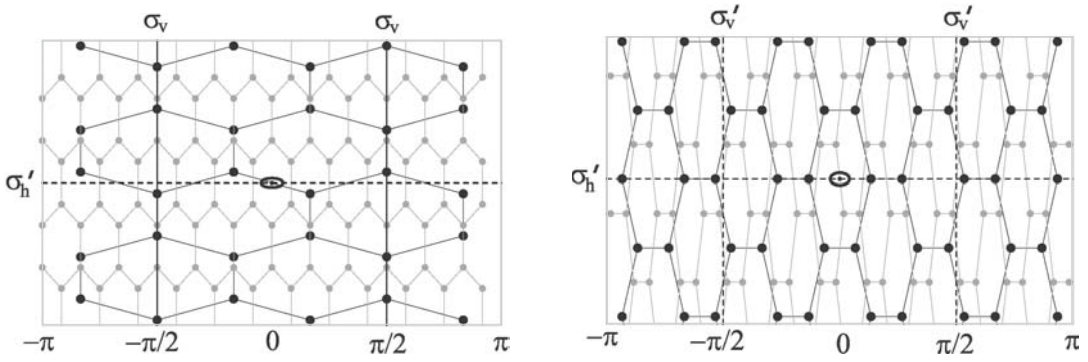

Fig. 1. Stable configuration of $\mathcal{Z}\mathcal{Z}_3$ and $\mathcal{A}\mathcal{A}_5$. On the unfolded double-layer (atoms are plotted in the φ-z coordinates) horizontal axis is at $\odot$, and mirror planes, vertical $\sigma_{\rm v}$ and $\sigma_{\rm h}$ horizontal (glide $\sigma'_{\rm v}$ and roto-reflection $\sigma'_{\rm h}$) planes are at solid (dashed) lines. Black and gray plots correspond to inner and outer shell.

the following full symmetry groups of CDWCNs:

$$\boldsymbol{L}_{\mathcal{C}} = \boldsymbol{T}_Q^R(A)\boldsymbol{D}_N = \boldsymbol{L}Q_P2, \boldsymbol{L}Q_P22 \text{ (LG family 5)}; \tag{2}$$

$$\boldsymbol{L}_{\mathcal{A}\mathcal{A}_5} = \boldsymbol{T}_c(a_0)\boldsymbol{S}_{10} = \boldsymbol{L}\bar{5}c \text{ (LG family10)}; \tag{3}$$

$$\boldsymbol{L}_{\mathcal{Z}\mathcal{Z}_9} = \boldsymbol{T}_c(\sqrt{3}a_0)\boldsymbol{S}_{18} = \boldsymbol{L}\bar{9}c \text{ (LG family10)}; \tag{4}$$

$$\boldsymbol{L}_{\mathcal{Z}\mathcal{Z}_n} = \boldsymbol{L}_{\mathcal{A}\mathcal{A}_n} = \boldsymbol{T}(A)\boldsymbol{D}_{Nd} = \boldsymbol{L}\bar{N}m \text{ (LG family9)}. \tag{5}$$

Here, $\boldsymbol{L}_{\mathcal{C}}$ denotes the groups of CDWCNs with a chiral wall, and $\boldsymbol{T}_c$ is yz-glide plane generated by $\sigma'_{\rm v} = (\sigma_{{\rm v}y}|A/2)$. The group parameters Q, R, N and A are given in Table 1. In the international notation, P is divisible by N, and $P = N(R^{\phi(Q/N)-1} \pmod{Q/N})$. As a consequence of symmetry, the conserved quantum numbers are quasi momentum k, angular momentum m, and parities. They are used to label irreducible representations in the form ${}_k\Gamma^{\Pi}_m$: U-parity is given by $\Pi = \pm$, while Γ is A (or B) for the one-dimensional representations even (odd) with respect to vertical mirror plane, and E and G for two- and four-dimensional representations. The isogonal point groups of $\boldsymbol{L}_{\mathcal{C}}$ and $\boldsymbol{L}_{\mathcal{Z}\mathcal{Z}}$ and $\boldsymbol{L}_{\mathcal{A}\mathcal{A}}$ are:

$$\boldsymbol{P}_{\mathcal{C}} = \boldsymbol{D}_Q, \quad \boldsymbol{P}_{\mathcal{Z}\mathcal{Z}} = \boldsymbol{P}_{\mathcal{A}\mathcal{A}} = \boldsymbol{D}_{Nd}. \tag{6}$$

While in SWCN the principle axis of the isogonal point groups is of high order, in the considered 318 CDWCNs it takes the values $Q = 1, 2, 3, 5, 9, 14$ (in 187, 88, 21, 9, 9 and 4 cases respectively). Whenever at least one wall is achiral, the resulting roto-translational group is symmorphic. Since the isogonal group of the achiral pairs is $\boldsymbol{D}_{Nd}$ with odd N, it contains spatial inversion which excludes simultaneous Raman and infrared (IR) activity.

The simulation package *POLSym* (E) fully implements the modified group projector technique [16] for the line groups, enabling substantial reduction of the eigen problem of the dynamical matrix $\mathcal{D}$. For each $|\mu|$-dimensional irreducible representation D^{μ} only $3|\mu|Y$-dimensional submatrix is extracted from $\mathcal{D}$ and diagonalized. Here, Y is the number of orbits of CDWCN, *i.e.* the minimal number of atoms that generate CDWCN tube by symmetry transformations. Skipping details on the orbits and

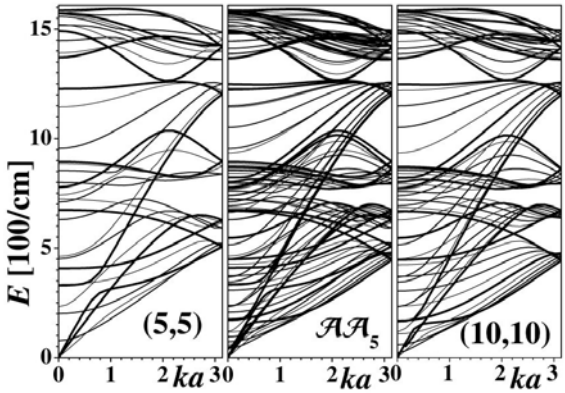

Fig. 2. Phonon dispersions of (5,5) (left), (10,10) (right) and CDWCN $\mathcal{A}\mathcal{A}_5$ (middle). The thickness of the bands corresponds to the quantum number m (modulo range $[-2,2]$ of m in $\mathcal{A}\mathcal{A}_5$), to enable comparison.

atomic coordinates, we note only that the CDWCNs symmetry is reduced with respect to the SWCNs one. The symmetry breaking [8] is manifested as the increased, tube dependent number of orbits, in contrast to the single orbit SWCNs. In view of this, the highly symmetric configurations, *e.g.* $\mathcal{A}\mathcal{A}_5$ or $\mathcal{Z}\mathcal{Z}_9$ with 3 orbits each (in general, $\mathcal{A}\mathcal{A}_{5n}$ has $2n+1$ and $\mathcal{Z}\mathcal{Z}_{9n}$ for $n > 1$ has $4(n+1)$ orbits), or (54,0)@(45,27), (30,30)@(55,10) are particularly convenient in calculations. On the contrary, there are many-orbit CDWCNs like (7,3)7@8 with more than 2000 orbits, for which the calculations are much robust then for SWCNs [18].

The dynamical matrix $\mathcal{D}$ is constructed as follows: For atoms α and β laying in different layers, the corresponding 3×3 sub-matrix $\mathcal{D}^{\alpha}_{\beta}$ is Hessian $\frac{\partial^2 v(\boldsymbol{r}_\alpha - \boldsymbol{r}_\beta)}{\partial x_i^\alpha \partial x_j^\beta}$ of the Lenard-Jones potential [15] (it gives the best matching with the measured Raman spectra). For the pair of atoms of the same layer $\mathcal{D}^{\alpha}_{\beta}$ is built up by use of the graphite force constants [17]; these are adjusted to the cylindrical geometry [18] dynamically (to reproduce forces changed due to the folding) and kinematically (to accommodate the

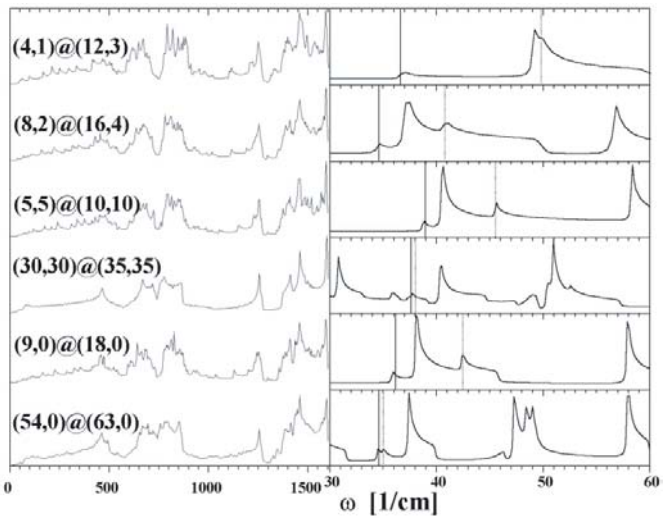

Fig. 3. Phonon density of states. Left: entire frequency range. Right: Enlarged low frequency region, with solid and dashed line denoting LRL and TWRL mode peaks.

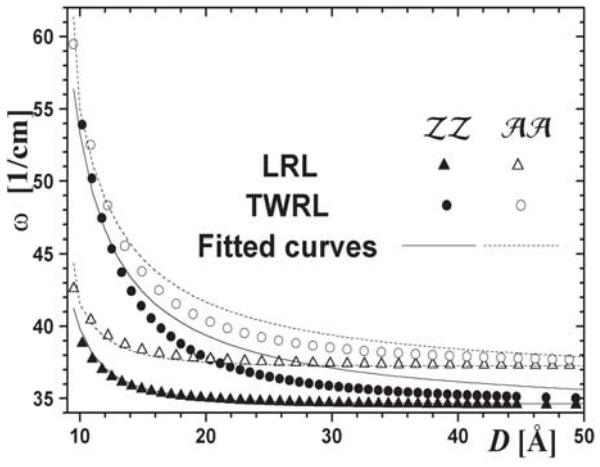

Fig. 4. Calculated and fitted by (7) frequencies of LRL and TWRL modes a functions of the tube diameter.

rotation sum rule). The inter-layer interaction is much weaker than the intra-layer one.

Due to the dominant intra-layer interaction, the CDWCN phonon energies are basically the perturbed energies of the isolated SWCN constituents (Fig. 2). This is helpful in the case of two modes of the isolated walls with the same quantum numbers, energetically separated from the other modes of the same type. Such a pair of the modes yields perturbatively a pair of CDWCN's modes. For instance, the pair of the radial breathing modes, one totally symmetric mode from each layer, gives two (out-of-phase and in-phase) breathing like modes of CDWCNs [6] (our results on these modes agree with the valence force fields ones). Of course, observed mixing with the other modes is neglected within this simple scheme.

There are four acoustic modes, longitudinal (LA), twisting (TWA) and two-fold transversal (TA). The corresponding branches are linear in k; their slope is close to that of SWCNs, giving the sound velocities: $v_{\mathrm{TA}} = 9.54$ km/s, $v_{\mathrm{LA}} = 20.64$ km/s and $v_{\mathrm{TC}} = 15.18$ km/s. Variations between different CDWCNs is within 1%.

The pair of LA modes of the walls are mixed to give one LA mode of CDWCN and the mode in which the walls move along the z-axis in opposite direction. This longitudinal vibration of the rigid layers will be denoted as LRL. Analogously, the twisting modes of both walls are mixed to give TWA and TWRL modes, in which rigid layers rotate in and out of phase. The acoustic and the corresponding rigid layers modes are assigned by the same line group irreducible representation: LA and LRL by ${}_0A_0^-$, TWA and TWRL by and ${}_0B_0^-$ (representations A_{2u} and A_{2g} of $\boldsymbol{D}_{Qd}$) for tubes with both achiral walls, and all by ${}_0A_0^-$ (for Q being 1, 2 and greater than 2 this is the representation B, B_1 and A_2 of the isogonal group $\boldsymbol{D}_Q$, respectively) for other CDWCNs. Hence, TRL and LRL modes are IR active, while TWRL is IR active for tubes with at least one chiral wall. In these cases they give intensive spectral lines since both TRL and TWRL modes correspond to singularities [19] in the phonon density of states (DOS), Figure 3.

In all these modes the interaction of the walls couples the layers acoustic modes of the same type, raising the frequencies from the exact zero (in SWCN) to approximately 40 cm^{-1}, Figure 4. Perturbation theory approximately relates frequencies and diameters:

$$\omega(D) = \omega_{\mathrm{DWCN}}^{\mathrm{RL}} \sqrt{\frac{(D+\delta^{\mathrm{RL}})(D-\frac{\Delta_{\mathrm{DWCN}}}{2})}{(D-\Delta_{\mathrm{DWCN}})D}}. \qquad (7)$$

Here, Δ is the difference of the walls diameters ($\Delta_{\mathcal{ZZ}} = 7$ Å and $\Delta_{\mathcal{AA}} = 6.78$ Å), while $\omega_{\mathrm{DWCN}}^{\mathrm{RL}}$ and $\delta_{\mathrm{DWCN}}^{\mathrm{RL}}$ are the fitting constant depending on the coupling: $\delta^{\mathrm{LRL}} = -4$ Å, $\delta^{\mathrm{TWRL}} = 4/3$ Å and $\omega_{\mathcal{ZZ}}^{\mathrm{LRL}} = 34.7$ cm^{-1}, $\omega_{\mathcal{ZZ}}^{\mathrm{TWRL}} = 33.8$ cm^{-1}, $\omega_{\mathcal{AA}}^{\mathrm{LRL}} = 37.4$ cm^{-1}, $\omega_{\mathcal{AA}}^{\mathrm{TWRL}} = 36$ cm^{-1}.

These results nicely agree with the predictions and measurements of the telescoping [8–11] of the walls (RL frequencies found with Van der Waals potential [10] are slightly higher for $\mathcal{AA}$ tubes, and lower for $\mathcal{ZZ}$ ones). The conclusions on the IR activity of LRL and TWRL modes and calculated frequencies may be combined in order to get a simple experimental test of the effect. Further, characterization of the samples of double-wall tubes is enabled; unlike only diameter dependent breathing-like Raman active modes, the proposed IR measurements of RL modes are chirality sensitive, as well. In the large diameter limit LRL and TWRL modes become the degenerate lowest A point mode of graphite [20] (below 40 cm^{-1}), with the adjacent graphene layers vibrating out of phase, rigidly and in plane. This limit differs for $\mathcal{AA}_n$ and $\mathcal{ZZ}_n$ tubes, due to the different stacking of the layers (Fig. 1). The limiting TRL and TWRL frequencies $\omega_{\mathrm{DWCN}}^{\mathrm{RL}}$ in (7) are not exactly degenerate due to the approximations incorporated in (7) and restricted fitting data base.

References

1. S. Iijima, Nature (London) **354**, 56 (1991)
2. D.E. Luzzi, B.W. Smith, in *Science and Application of Nanotubes*, edited by D. Tomańek, R.J. Enbody (Kluwer, New York, 2000), p. 67
3. B.W. Smith, D.E. Luzzi, Chem. Phys. Lett. **321**, 169 (2000); K. Hirahara *et al.*, Phys. Rev. Lett. **85**, 5384 (2000)
4. R.R. Bacsa *et al.*, Chem. Phys. Lett. **323**, 566 (2000); W.Z. Li *et al.*, Chem. Phys. Lett. **368**, 299 (2002)
5. S. Bandow *et al.*, Chem. Phys. Lett. **337**, 48 (2001); J.M. Benoit *et al.*, Phys. Rev. B **66**, 073417 (2002); S. Bandow *et al.*, Phys. Rev. B **66**, 075416 (2002); R.R. Bacsa, A. Peigney, Ch. Laurent, P. Puech, W.S. Bacsa, Phys. Rev. B **65**, 161404 (2002)
6. V.N. Popov, L. Henrard, Phys. Rev. B **65**, 235415 (2002)
7. M. Damnjanović *et al.*, Phys. Rev. B **60**, 2728 (1999)
8. M. Damnjanović *et al.*, Eur. Phys. J. B **25**, 131 (2002); T. Vuković *et al.*, Physica E **16**, 259 (2003)
9. J.-C. Charlier, J.-P. Michenaud, Phys. Rev. Lett. **70**, 1858 (1993)
10. A. Kolmogorov, V. Crespi, Phys. Rev. Lett. **85**, 4727 (2000)
11. J. Cumings, A. Zettl, Science **289**, 602 (2000); M. Yu *et al.*, J. Phys. Chem. B **104**, 8764 (2000)
12. I. Milošević *et al.*, *Poly*mer *sym*metry simulation package: Chap. XIV in *Quantum Mechanical Simulation Methods in Studying Biological Systems*, edited by D. Bicout, M. Field (Springer-Verlag, Berlin 1996)
13. I. Milošević, M. Damnjanović, Phys. Rev. B **47**, 7805 (1993)
14. H. Abud, G. Sartori, Ann. Phys. **150**, 307 (1983)
15. R. Saito *et al.*, Chem. Phys. Lett. **348**, 187 (2001)
16. M. Damnjanović *et al.*, J. Phys. A **33**, 6561 (2000)
17. R.A. Jishi *et al.*, Chem. Phys. Lett. **209**, 77 (1993)
18. E. Dobardžić *et al.*, Phys. Rev. B **68**, 045408 (2003)
19. T. Vuković *et al.*, Phys. Rev. B **65**, 045418 (2002)
20. A. Jishi, G. Dresselhaus, Phys. Rev. B **26**, 4514 (1982)